



Article

Experimental Investigation of Unidirectional Glass-Fiber-Reinforced Plastics under High Strain Rates

Sören Bieler ^{1,*} , Sebastian Haller ², Robert Brandt ² and Kerstin Weinberg ¹

¹ Chair of Solid Mechanics, Department of Mechanical Engineering, University of Siegen, Paul-Bonatz-Str. 9–11, 57076 Siegen, Germany; kerstin.weinberg@uni-siegen.de

² Chair of Material Systems for Lightweight Vehicle Construction, Department of Mechanical Engineering, University of Siegen, Am Eichenhang 50, 57076 Siegen, Germany; sebastian.haller@uni-siegen.de (S.H.); robert.brandt@uni-siegen.de (R.B.)

* Correspondence: soeren.bieler@uni-siegen.de; Tel.: +49-271-740-4644

Abstract: When a vehicle leaves the road, crash barriers stop it and prevent significant damage to the vehicle, its environment, and the occupants. Typically, such protection systems are made of simple steel, but fiber-reinforced composites can efficiently absorb and dissipate the impact energy at high-risk locations. In order to design such protective systems, material parameters under dynamic loading are necessary. Here, split Hopkinson pressure bar tests with unidirectional glass-fiber-reinforced epoxy of 58% glass fiber content are performed. The elastic response at strain rates between 300/s and 700/s in the loading direction parallel and perpendicular to the fiber is determined. From the measured data, a model of the time dependence of the elastic modulus is derived to enable the design engineer to lay out protective systems made of such GFRPs.

Keywords: glass-fiber-reinforced epoxy; crash test; split Hopkinson pressure bar; dynamic compression; composite material; high strain rates; energy absorption; material model

1. Introduction

For highly advanced crash-absorbing structures such as crash boxes in modern racing cars, reinforced materials, particularly unidirectional glass-fiber-reinforced plastics (GFRPs), are often used. Similarly, advanced guardrails, also called crash barriers, which are safety devices installed along roads and highways to prevent vehicles from leaving the roadway or colliding with dangerous obstacles, can be made of GFRPs. They are used to redirect or absorb the vehicle's impact energy to reduce the severity of accidents and to protect both the vehicle's occupants and other road users. Up to now, crash barriers have typically been made of sturdy materials such as steel or concrete. They are strategically placed in areas of increased accident risk, such as sharp curves, bridges, or steep slopes.

The choice of the crash barrier material depends on several factors, including the desired level of protection, cost, and environmental considerations. Steel crash barriers are widespread and often found on country roads, see Figure 1. Steel is commonly used for crash barriers due to its high strength and durability. It can effectively absorb and dissipate energy during an impact, reducing the severity of the impact. Steel crash barriers are often galvanized to increase their corrosion resistance and durability. Concrete crash barriers are used on highways and other high-speed roads. They usually consist of precast reinforced concrete elements joining a continuous barrier and provide excellent protection against vehicle intrusion and high-impact forces. Composite materials, such as fiber-reinforced polymers, are becoming increasingly popular in crash barrier applications because they offer a combination of high strength, being lightweight, and corrosion resistance. The specific choice of crash barrier material depends on the project's specific requirements, including the desired level of protection, budget constraints, and local regulations.



Citation: Bieler, S.; Haller, S.; Brandt, R.; Weinberg, K. Experimental Investigation of Unidirectional Glass-Fiber-Reinforced Plastics under High Strain Rates. *Appl. Mech.* **2023**, *4*, 1127–1139. <https://doi.org/10.3390/applmech4040058>

Received: 20 September 2023

Revised: 13 October 2023

Accepted: 19 October 2023

Published: 26 October 2023



Copyright: © 2023 by the authors. Licensee MDPI, Basel, Switzerland. This article is an open access article distributed under the terms and conditions of the Creative Commons Attribution (CC BY) license (<https://creativecommons.org/licenses/by/4.0/>).



Figure 1. Typical guardrails to keep vehicles on the road.

Since most fatal accidents occur on country roads, it is reasonable to use high-quality GFRP materials here. Furthermore, hybrid constructions are particularly desirable for cost reasons, i.e., constructions made of a steel and GFRP combination. To design such structures that protect against car impact, strain-rate-dependent material data for GFRPs are needed. That motivated us to investigate GFRPs at high strain rates of up to 700/s in this work.

For the impact experiments of our GFRP specimens, we use the split Hopkinson pressure bar (SHPB). The SHPB is a common experimental device for determining the dynamic material properties under moderate and high strain rates [1,2]. Hereby, the strain rate $\dot{\epsilon}$ is a measure of how quickly the material is compressed or stretched, i.e., it quantifies the change of strain ϵ per unit of time (1/s). Knowing the response helps us to understand and predict the behavior of materials under a high-speed impact, allowing for the design and optimization of structures and materials that can withstand such loading conditions.

Several authors have already studied the dynamic behavior of GFRP materials, e.g., [3–9]. Most investigations focused on the failure modes and strengths at higher strain rates. While [3] concentrated on the effect of different fiber orientations, the works [8,9] only present experiments on a specimen with fiber orientation in the loading direction. An increase in Young's modulus was found. Different fiber volume fractions in their samples were considered in [9]. An increasing stress–strain curve was also observed by [4] by raising the strain rates for different fiber volume fractions during the tests. In [6], specimens similar to ours in terms of fiber volume fraction were tested. They noticed an increase in Young's modulus with an increasing strain rate for both parallel and orthogonal fiber orientation. Paper [7] deals with investigating the compressive impact properties of GFRP utilizing a servohydraulic apparatus. This method allows experiments to be performed at medium strain rates (up to approx. 100/s). The authors specify a dynamic Young's modulus E_{dyn} in their work. Since all investigated GFRP materials differ concerning the matrix material and the fiber material and its volume fraction, the comparability of experimental data is difficult. Here, we present the data collected from the literature and compare them to our results in our discussion.

Polymeric material behavior usually has a strong dependence on the strain rate. Thus, knowledge gained from the classic tensile tests can only be used to a limited extent to design materials subjected to impact loads. Typically, vehicles crash into the guardrails at speeds of 50 to 100 km/h, which results in strain rates of about 500/s. Therefore, we investigate three different strain rates in this range to characterize the dynamic behavior of GFRPs. From the results, an effective rate-dependent material model is derived. To our knowledge, such detailed information on GFRP materials has not yet been given.

The remainder of the paper is organized as follows: In Section 2, the experimental setup of the SHPB, as well as the specimen design and its material components, are described. Our specimens have two configurations that differ in the orientation of their fibers, namely parallel and orthogonal to the loading direction (GFRP \parallel , GFRP \perp). Section 3 presents the dynamic experiments performed on the GFRP specimens. Strain rates of up to 700/s are evaluated. In Section 4, we derive a constitutive model for time dependency of the elastic modulus. A comparison with other works on GFRP is given in Section 5, and Section 6 provides the conclusion.

2. Specimen and Experimental Setup

The specimens were cut from unidirectional GFRP plates. To manufacture such plates, the raw material of the unidirectional GFRP was available as tape. It consisted of an epoxy resin matrix and glass fibers with a diameter of 20 μm , while the plate's fiber volume fraction V_f reached 58%. The tape material was provided by the company MUBEA Attendorn. A specific number of tapes with a thickness each of 600 μm were pressed inside a hot pressing tool under a pressure of four bar and temperature up to 230 $^{\circ}\text{C}$. After the consolidation, cylindrical specimens were cut out using a waterjet process. Since waterjet cutting only produces a rough shape of the specimens, they are subsequently processed further. CNC turning ensures the roundness of the cylindrical specimen, and grinding processes guarantee a perfect surface of the specimen. Two types of cylindrical specimens with length l and diameter d were prepared. The first type of specimen was cut so that the fibers were oriented parallel to the cylinder axis, see Figure 2a. These specimens are referred to as GFRP \parallel in the following. The second specimen type was cut so that the fibers were oriented perpendicularly to the cylinder axis, see Figure 2b. These types of specimen are named GFRP \perp .

In this study, the two limiting cases of loads regarding the fiber orientation (perpendicular and parallel) are considered; both are needed to map the direction-dependent (orthotropic) material behavior of unidirectional fiber-reinforced material. We note that a cylindrical GFRP specimen with a diameter of 10 mm contains approximately 145,000 glass fibers.

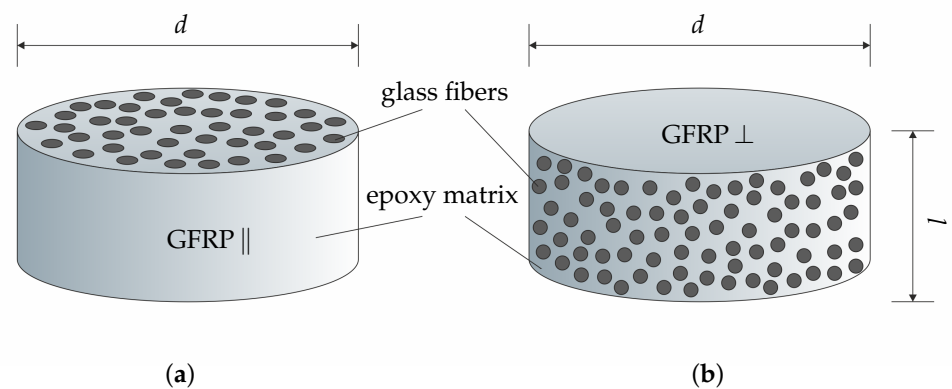


Figure 2. Two different types of GFRP specimen, with the fibers aligned (a) parallel and (b) perpendicular to the applied force. The fiber matrix consists of epoxy resin.

2.1. Static Properties of the Tested GFRP

For reference and later modeling of the effective material behaviour, we started by determining the modulus of elasticity for the GFRP \parallel and the GFRP \perp specimen under static loading. The elastic modules of the components, namely the glass fibers and the epoxy matrix, are known as 72 GPa and 4 GPa, respectively. The composite's modulus can

then be approximated using the Voigt and Reuss rules of mixtures, which give an upper and a lower bound for the homogenized modules of elasticity [10].

$$E_{\text{low}} = \left(\frac{f_M}{E_M} + \frac{f_F}{E_F} \right)^{-1} \tag{1}$$

$$E_{\text{up}} = f_F E_F + f_M E_M \tag{2}$$

Here, E_F and E_M refer to the fibers' and the matrix material, and f_F and $f_M = 1 - f_F$ denote the corresponding volume fractions. We have $f_F = 0.58$ here.

In our setting of unidirectional fibers, we identify the Voigt modulus E_{up} with the elastic modulus of the GFRP \parallel specimen and the Reuss modulus E_{low} with the GFRP \perp material. In that way we determine:

$$\begin{aligned} E_{\text{stat}} &= 43.44 \text{ GPa} && \text{for GFRP } \parallel \\ E_{\text{stat}} &= 8.85 \text{ GPa} && \text{for GFRP } \perp \end{aligned}$$

We note that these values are in line with the elastic modules given by the manufacturer (about 45 GPa) and some in-house uniaxial compression tests.

2.2. Split Hopkinson Pressure Bar

Young's modulus at high strain rates, also known as the dynamic modulus of elasticity E_{dyn} , refers to the modulus of the material's elasticity under rapid loading conditions. When a material is subjected to a high rate of straining, such as during impact or explosions, its behavior can differ significantly from that under static or low strain rate conditions. E_{dyn} is typically determined through specialized testing techniques, such as SHPB experiments or high-speed tensile testing. These tests load the material specimen dynamically and measure its resulting stress-strain response.

In the SHPB setup of [11], two long bars are aligned along their axis, and the material specimen is placed between them, see Figure 3. Both bars have a circular cross-section and are usually of the same length. The geometry of the bars and specimens used here can be found in Table 1. The bars in our testing setup are made of steel. A striker, typically made from the same material and diameter, is accelerated by a gas gun, and when it hits the front face of the first bar (incident bar), a stress pulse is induced. This pressure wave travels through the incident bar and reaches the specimen at its end. Because the specimen is small, it acts in the same way as an interface. A part of the wave is reflected, and the rest is transmitted into the second bar (transmission bar).

The reflection results from the impedance mismatch between the bar and the specimen. The impedance Z measures how effectively a wave can propagate in a medium and is determined by the material density ρ and propagation velocity c , cf. Equation (3). The impedance mismatch between the selected bar material and specimen material may result in insufficient impulse transmission. If the impedance difference is very high, almost the entire wave is reflected at the interface between the incident bar and the specimen. A correspondingly weak or no pulse is then measured at the transmission bar. For this reason, the bars used must be adapted to the material to be tested. For example, bars made of PMMA are used for soft materials [12]. During the transition from one medium to another, the cross-sectional area over which the wave is transmitted also plays a role. For this reason, the impedance is also listed in relation to the cross-sectional area of the bars,

$$Z = \rho c \quad \text{and} \quad \hat{Z} = \rho c A = \rho c \frac{\pi d^2}{4}. \tag{3}$$

The incident, the reflected, and the transmitted wave are measured with strain gauges placed in the center of the corresponding bars. In our experiments, the waves are recorded at a sampling rate of 10^{-6} s^{-1} by the HBM GEN7t data acquisition system equipped with two bridge cards, type GN411. Each bridge card is supplied by four channels, with each

channel able to measure up to 1 MS/s. Wheatstone bridges in a full-bridge configuration are used (HBM 3/350 XY31), with a resistance of $350.0 \Omega \pm 0.30\%$ and a gauge factor of $2.0 \pm 1.0\%$. The laboratory has a constant temperature of 20°C .

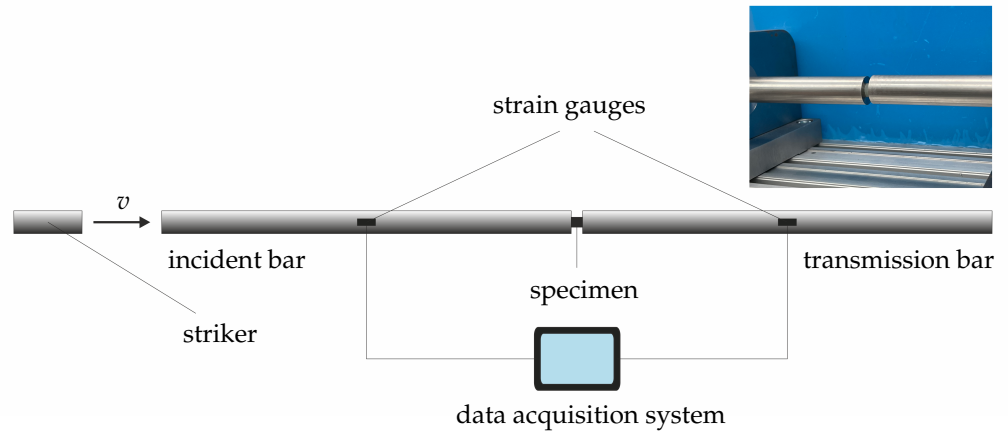


Figure 3. The split Hopkinson pressure bar setting with the specimen being placed between the incident bar (IB) and transmission bar (TB). A striker hits the incident bar with a velocity v , and the change in the material wave is recorded with two strain gauges.

Table 1. Geometric and material specific values.

	IB	TB	Striker	GFRP	GFRP ⊥
material	steel	steel	steel	glass/epoxy	glass/epoxy
d (mm)	20	20	20	10	10
l (mm)	1800	1800	300	3–5	3–5
ρ (kg/m ³)	7850	7850	7850	2020	2020
E (GPa)	210	210	210	43.44	8.85
c (m/s)	5100	5100	5100	4690	2093
Z (kg/m ² μs)	40.04	40.04	40.04	9.47	4.23

2.3. Basic Equations for the SHPB Experiment

The SHPB experiment assumes that a one-dimensional wave propagates through the bars and the specimen following the equation

$$c^2 \frac{\partial^2 u}{\partial x^2} = \frac{\partial^2 u}{\partial t^2} \tag{4}$$

where u is the displacement and $c = \sqrt{E/\rho}$ is the wave speed of the bar material. During the experiment, three strain pulses are measured: the incident pulse ϵ_I , the reflected ϵ_R , and the transmitted pulse ϵ_T . Then, the strain in the specimen ϵ_s , its strain rate $\dot{\epsilon}_s$, and stress σ_s are calculated as follows:

$$\dot{\epsilon}_s = -2 \frac{c}{l_s} \epsilon_R \tag{5}$$

$$\epsilon_s = -2 \frac{c}{l_s} \int_{t_0}^t \epsilon_R dt \tag{6}$$

$$\sigma_s = \frac{E_b A_b}{A_s} \epsilon_T \tag{7}$$

Here, A and l are the cross-section area and the length of bar (index “ b ”) and specimen (index “ s ”), respectively. For a detailed derivation, we refer to [13–15]. For the evaluation of the experiments, a period of stress equilibrium and a constant strain rate $\dot{\epsilon}$ are

presumed. The stress equilibrium in the sample can be reached more reliably when using thin specimens [16,17]. The necessary conditions are discussed in the following.

2.4. Prerequisites of the SHPB Experiment

The specimen’s geometry has to be chosen so that its deformation is uniform and friction during deformation and inertia effects are minimized. This condition can be achieved by a length-to-diameter ratio of 2:1 to 3:1, cf. [13]. Our specimens have $l/d \approx 0.3$ to 0.5 and are exactly in this range. Lubricant is applied between the specimen’s surfaces and the bars to reduce the friction effects, cf. [18]. To achieve a stress equilibrium, the stress state described by the lateral force F has to be equal at both surfaces of the specimen. It is challenging to meet this condition, and therefore, a factor for the stress equilibrium R is introduced, cf. [19]. In Equation (8), F_1 represents the force at the front side of the specimen, and F_2 is the force at the back end of the specimen. Both are evaluated from the measured wave signals of the incident and transmission bars. In our experiments, an R of less than or equal to 10% was chosen as being acceptable, see Figure 4.

$$R = \left| \frac{\Delta F(t)}{F_m} \right| = 2 \left| \frac{F_1 - F_2}{F_1 + F_2} \right| \leq 0.1 \tag{8}$$

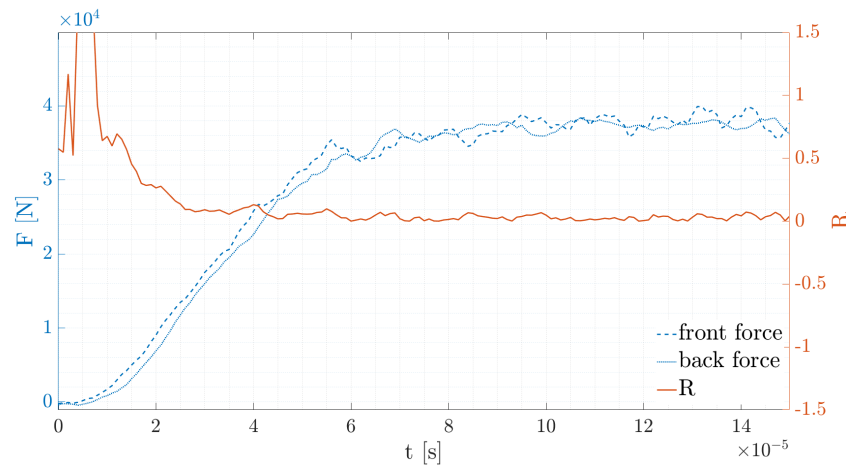


Figure 4. Forces on the front side (dashed line) and back side (dotted line) of the specimen as well as the R (solid line).

We note that the wave signals measured at the centered strain gauges in steel bars are assumed to be the signals that arrive at the interface of the bars and specimen. This assumption can be made due to the low dispersions in metal bars. This concept does not apply when testing with polymeric bars where the recorded signals need to be corrected, cf. [20]. The specimen’s strain, strain rate, and stress can be calculated with the Equations (5) to (7) from the measured data. The stress–strain curves presented here were calculated from the average values measured on the plateau of the reflected pulse.

3. Experimental Results

For reproducible results, the SHPB experiments have to be performed multiple times. A representative incident pulse must be created to obtain a suitable signal in the experiment, which requires some adjustment in the SHPB setup at first.

3.1. Pulse Shaping

The length of the pulse can be adjusted by the striker length, whereas the impact velocity controls its amplitude, cf. [12]. Our striker velocities vary between 4 m/s and 8 m/s, which results in three different strain rates. Moreover, a pulseshaper is used to modify the pulse profile and also diminishes the oscillations of the wave, cf. [21]. These pulseshapers are thin lead discs with a diameter of 8 mm and a thickness of 0.2–0.3 mm;

they increase the pulse's rise time to its maximum. Discs made of lead have already been used with aluminum bars and have proven to be suitable pulse-shapers [22]. In addition, high spectrum frequencies are filtered out of the signal (low-pass filter), resulting in a smoother pulse, cf. [23,24]. Figure 5a shows the application of the pulse-shaper disc to the impact surface of the incident bar. In Figure 5b, both the plain incident signal and the pulse-shaper-modified signal are shown.

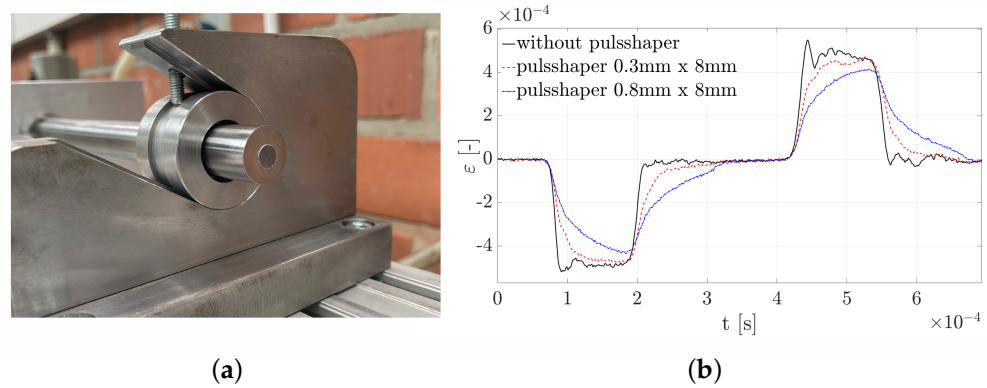


Figure 5. Pulse-shaper made of lead applied to the incident bar surface (a) and the changing shape of the incident signal due to pulse-shapers (b).

3.2. Experimental Evaluation

The signals recorded by the strain gauges are exported and analyzed in Matlab. With these raw data, the stress–strain behavior can be calculated by using Equations (6) and (7). A set of five specimens were tested for each experiment. Three different strain rates were investigated for both fiber orientations ($\approx 300/s$, $500/s$, $700/s$). In total, 30 measurements were performed. Figure 6 shows the stress–strain curves of both specimen types at different strain rates.

Every specimen was tested only once. Thus, erroneous measurements can be ruled out due to possible changes in the internal material structure. The results are shown in Figure 6a for the specimens with fibers in the loading direction and in Figure 6b for the specimens with fibers perpendicular to the loading direction. The individual stress–strain curves show the mean values at each strain rate.

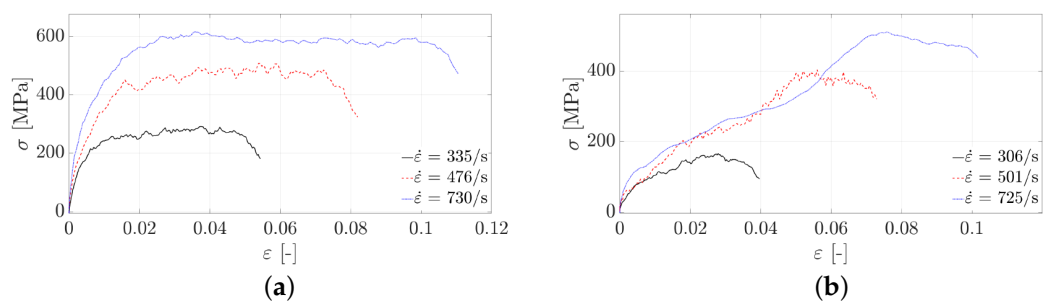


Figure 6. Stress–strain curves of GFRP \parallel (a) and GFRP \perp (b) at different strain rates.

The specimens with parallel fiber orientation show higher stresses than the specimens with the perpendicular alignment of the fibers. In the GFRP \parallel specimens, the fibers are stressed in the axial direction as with bars. In addition, they are held in position due to the matrix material. Therefore, this fiber orientation has a much higher stiffness than the one used for the second load case. When specimens with perpendicular fiber orientation are loaded, the fibers can move against each other more easily. Accordingly, equal strains can be achieved by lower stresses. This clearly corresponds to the evaluation of the static elastic modulus above.

By analyzing the stress–strain data, the dynamic modulus of elasticity E_{dyn} can be estimated for the material under the appropriate strain rate. For this purpose, the stress–strain curve for each specimen is calculated using Equations (5) to (7). Then, a regression is performed for the linear increase in the stress–strain curve (up to about 0.5%). This results in the specific elastic modules; the underlying data are presented in Table 2.

Table 2. Experimentally obtained values for the specimens’ strain with a constant strain rate, the average strain rate, and the average stress maximum according to Equations (5)–(7).

	ϵ_s (-)	$\dot{\epsilon}_s$ (1/s)	σ_s (MPa)
GFRP	0.007..... 0.061	335	291.57
GFRP	0.008..... 0.088	476	508.28
GFRP	0.012..... 0.121	730	614.72
GFRP ⊥	0.005..... 0.042	306	166.05
GFRP ⊥	0.007..... 0.078	501	403.69
GFRP ⊥	0.011..... 0.112	725	511.63

We observe that the elastic modulus increases with increasing strain rate. Table 3 shows the averaged determined dynamic elastic modules for the different strain rates.

Table 3. Module of elasticity of unidirectional glass-fiber-reinforced epoxy with a fiber volume of 58% for different strain rates and two fiber orientations.

		GFRP	GFRP ⊥
E_{stat}	(GPa)	43.4	8.8
$E_{dyn}(\dot{\epsilon} \approx 300/s)$	(GPa)	46.6	13.4
$E_{dyn}(\dot{\epsilon} \approx 500/s)$	(GPa)	50.8	17.3
$E_{dyn}(\dot{\epsilon} \approx 700/s)$	(GPa)	53.5	21.1

4. Material Model for High Strain Rates

The goal of our investigation was not only to measure the increase in the elastic modulus E_{dyn} under impact but also to provide the design engineer with a tool for dimensioning GFRP collision barriers. The stiffness at high strain rates refers to the ability of the material or structure to dissipate and absorb energy when subjected to rapid loading. To account for such a situation in a numerical computation, a material model for the effective response of the CFRP material under different strain rates is needed.

For this purpose, we refer to rheological models as combinations of elastic springs (with modulus E) and dashpots (with characteristic times τ). The latter ones account for the time dependence of the response and are related to the strain rate $\dot{\epsilon}$. In Figure 7, the simplest of such a model, a linear standard body, is displayed.

Such rheological models are known from viscoelasticity where each spring–dashpot element represents a relaxation process with a specific relaxation time τ . Here, we derive the constitutive relation in an analogous manner to obtain

$$E(\dot{\epsilon}) = E_{stat} + \sum_{i=1}^3 \Delta E_i \exp\left(-\frac{\dot{\epsilon}}{\dot{\epsilon}_i^{ref}}\right) \tag{9}$$

with $\dot{\epsilon}_i^{ref} = \epsilon^{ref} / \tau_i$ being a characteristic strain rate; ΔE_i is the corresponding increase in stiffness. We use the values measured in our experiments and set $\epsilon_{ref} = \epsilon_s$ etc., see Table 2. Such a model results in a $E(\dot{\epsilon})$ curve for GFRP || as displayed in Figure 8.

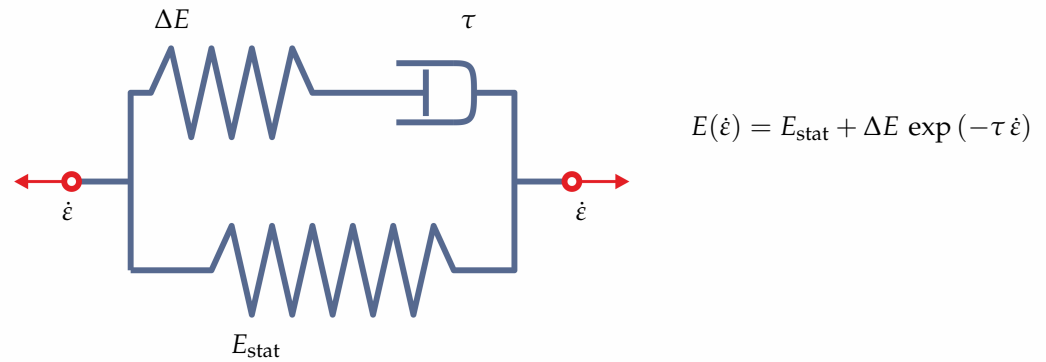


Figure 7. Combination of one spring–dashpot element combined with a basic spring to model a strain-rate-dependent elastic material $E(\dot{\epsilon})$.

Because the measured strain rates do not differ by orders of magnitude—compared to the full spectrum of possible rates—the model can be simplified by using just one spring–dashpot element, $N = 1$, with a mean value of τ . This corresponds to the model of Figure 7 and results in a basically identical $E(\dot{\epsilon})$ curve for GFRP \parallel . For GFRP \perp , the corresponding $E(\dot{\epsilon})$ curve is also displayed in Figure 8. \circ and \diamond indicate the measured values.

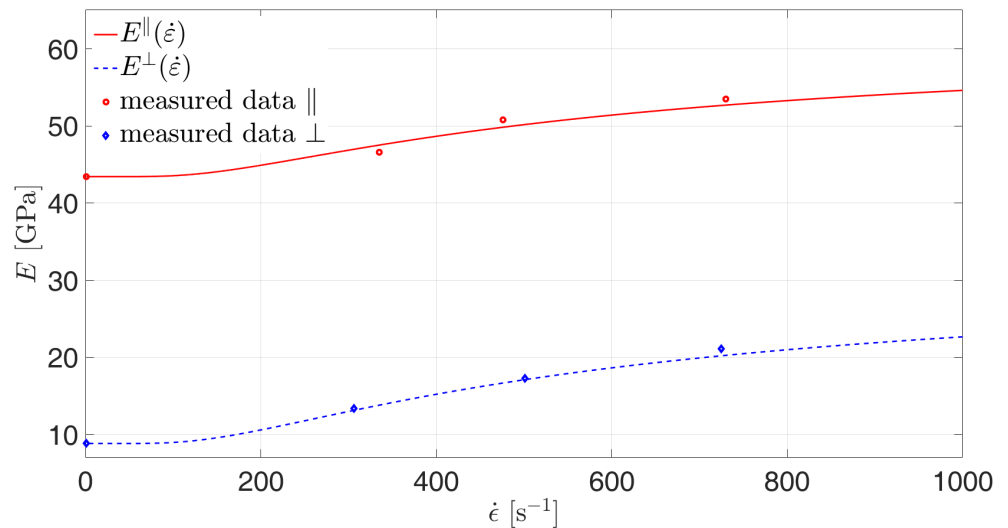


Figure 8. Model for the rate dependence of the elastic modulus $E(\dot{\epsilon})$ in GFRP \parallel and GFRP \perp .

The proper material parameters are crucial for the simulation of crash events. We refer to [25] where the authors pointed out that experiments must determine these data to simulate the crash event as accurately as possible. Thus, with a view to use the derived constitutive model in a commercial finite element program, we go one step further and express relation (9) as a function of time, $E(t)$. Such Prony series models are usually available, e.g., in ABAQUS and ANSYS, and are primarily used to model the viscoelastic behavior of materials. Here it reads

$$\begin{aligned}
 E(t) &= E_{\text{stat}} + \Delta E \exp(-t/\tau) \\
 &= E_{\text{stat}}(1 + \gamma_0 \exp(-t/\tau)) \quad \text{with} \quad \gamma_0 = \frac{\Delta E}{E_{\text{stat}}} .
 \end{aligned}
 \tag{10}$$

From the values above, we determine a reference strain of $\epsilon = 0.08$ and derive $\tau^{\parallel} = 177 \mu\text{s}$ and $\tau^{\perp} = 151 \mu\text{s}$ and

$$\begin{aligned} \gamma_0^{\parallel} &= 0.23 && \text{for GFRP } \parallel \\ \gamma_0^{\perp} &= 1.39 && \text{for GFRP } \perp \end{aligned}$$

The resulting time-dependent elastic modules $E(t)$ are displayed in Figure 9.

We conclude with two remarks. First, our model can only be used for strain rates below 1000/s, which are typically for car crashes and vehicle collisions [26]. The data do not allow extrapolation to higher strain rates. To extend the model to incidents such as explosions, further experiments are required, e.g., Taylor impact tests.

Second, we attribute all time dependency observed in high-strain-rate loading to viscoelastic effects. Of course, this is a simplification because other effects, such as inertia, may also contribute to the modified elasticity. However, it is justified by the benefit of a handy model for designing GFRP collision barriers.

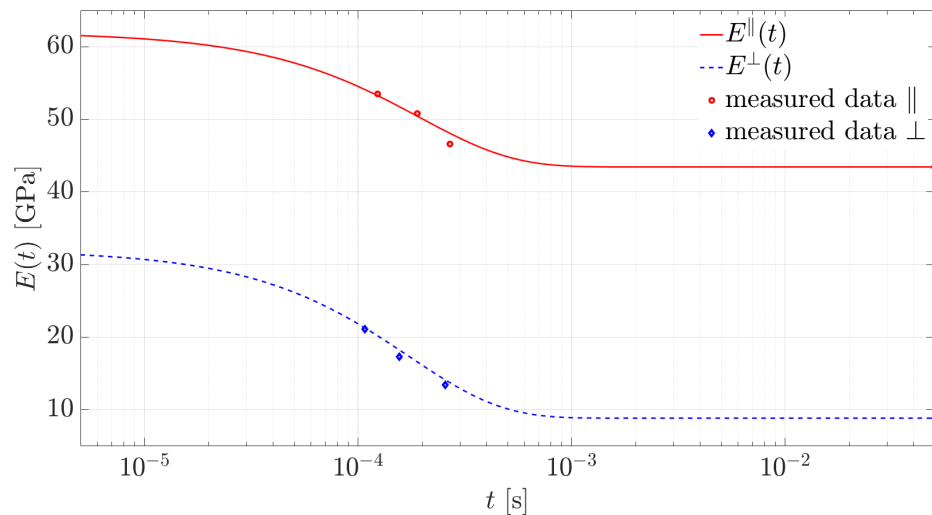


Figure 9. Time dependency of the elastic modulus $E(t)$ in GFRP \parallel and in GFRP \perp .

5. Discussion and Comparison with Other Experiments

Energy absorption at high strain rates is essential in various engineering applications where the ability to dissipate energy and protect against sudden dynamic loading events is critical. Materials with a high stiffness (and ductility) can absorb more energy before they fail. In that sense, the strain-rate sensitivity of a material refers to the increase in its stiffness under high rate loading. Such a material can be achieved through advanced manufacturing techniques, such as tailored forming processes or by incorporating energy-absorbing layers and inlets. Moreover, in [27], the authors state that a composite material (fiber-reinforced rubcrete in their case) provides a better energy absorption than, for example, a crash barrier made of pure concrete.

The dynamic measurements of the GFRP specimens show an increase in the stress–strain curves similar to other works, cf. [4,6,8,28]. Comparing the strain-rate-sensitive stress–strain behavior is complicated because there is no standard method for executing SHPB tests. In addition, the material compositions influence the results. The material’s behavior is influenced by several factors, such as the speed of the striker, the testing method, the fiber volume fraction V_f , the length-to-diameter ratio, and the matrix and fiber material. In addition, the specimen’s fiber direction must be considered. Therefore, Table 4 refers to the different polymer matrices with the fiber volume fractions V_f in a range between $0.46 < V_f < 0.60$ according to the individual authors. Our observed increase in the modulus of elasticity is in line with the results of these authors.

Table 4. Comparison of static and dynamic elastic modules experimental results determined by SHPB tests [4,6,9,28] and servohydraulic testing [7]; the values are not explicitly given but are derived from the data in the publication.

Source	V_f	Matrix Material	Fibers	E_{stat} (GPa)	E_{dyn} (GPa)	$\dot{\epsilon}$ (1/s)
here	0.58	epoxy resin		43.44	46.60	335
here	0.58	epoxy resin		43.44	50.80	476
here	0.58	epoxy resin		43.44	53.50	730
[4]	0.61	epoxy resin		-	36.50	620
[6]	0.46	epoxy resin		32.00	33.50	265
[7]	0.50	epoxy resin		24.79	38.25	85
[28]	0.54	epoxy resin		-	35.50	429
[28]	0.54	epoxy resin		-	37.25	702
[28]	0.54	epoxy resin		-	60.00	1031
[9]	0.60	Vinyl ester		37.50	48.50	1020
here	0.58	epoxy resin	⊥	8.85	13.40	306
here	0.58	epoxy resin	⊥	8.85	17.30	501
here	0.58	epoxy resin	⊥	8.85	21.10	725
[6]	0.46	epoxy resin	⊥	7.50	9.5	725
[28]	0.54	epoxy resin	⊥	-	25.25	265

6. Conclusions

In places where serious traffic accidents frequently occur, using crash barriers made of GFRP material is advisable. To dimension such structures, strain-rate-dependent materials are needed. In this work, dynamic compression tests were performed using the SHPB technique. GFRP specimens with different fiber orientations (parallel and orthogonal) were investigated. We found that the elastic modulus increases with increasing strain rate up to 19% for GFRP || and up to 58% for GFRP ⊥ at a strain rate of about 700/s in contrast to the static modules.

Additionally, a constitutive model for the time dependency of the elastic modulus was derived. It describes the material’s elasticity for strain rates up to 1000/s independent of the loading direction. This material model can be used in future finite element simulations regarding impact analyses, car crashes, and collision incidents.

Our obtained results were placed in the context of previously published work. Although a comparison is only possible to a limited extent due to the different kinds of methods and tested GFRP materials, we found a plausible match to our observations.

The time dependency of a material’s elasticity is essential in impact engineering, ballistics, automotive safety, and defense applications. It helps understand and predict the behavior of materials under a high-speed impact or explosive events, allowing for the design and optimization of structures and materials to withstand such loading conditions.

Author Contributions: Conceptualization, S.B., S.H., R.B., and K.W.; methodology, S.B. and K.W.; software, K.W. and S.B.; validation, R.B. and K.W.; formal analysis, K.W. and R.B.; investigation, S.B.; resources, S.H.; writing—original draft preparation, S.B. and S.H; writing—review and editing, S.B., R.B., and K.W.; visualization, S.B. and K.W; supervision, K.W.; project administration, R.B. and K.W. All authors have read and agreed to the published version of the manuscript.

Funding: This research received no external funding.

Institutional Review Board Statement: Not applicable.

Informed Consent Statement: Not applicable.

Data Availability Statement: The data supporting this study’s findings are available from the corresponding author upon reasonable request. The data are not publicly available due to privacy restrictions of the specimen’s manufacturer.

Conflicts of Interest: The authors declare no conflicts of interest.

Abbreviations

The following abbreviations are used in this manuscript:

SHPB	split Hopkinson pressure bar
GFRPs	glass-fiber-reinforced plastics
PMMA	polymethylmethacrylate

References

1. Owens, A.; Tippur, H. A tensile split Hopkinson bar for testing particulate polymer composites under elevated rates of loading. *Exp. Mech.* **2009**, *49*, 799–811. [[CrossRef](#)]
2. Zhao, J.; Knauss, W.; Ravichandran, G. Applicability of the time–temperature superposition principle in modeling dynamic response of a polyurea. *Mech. Time-Depend. Mater.* **2007**, *11*, 289–308. [[CrossRef](#)]
3. Amijima, S.; Fujii, T. Compressive Strength and Fracture Characteristics of Fiber Composites under Impact Loading. *Advances in Composite Materials*. In *Proceeding of the 3rd International Conference of Composite Materials, ICCM III, Paris, France, 26–29 August 1980*; pp. 399–413
4. El-Habak, A. Compressive resistance of unidirectional GFRP under high rate of loading. *Compos. Technol. Res.* **1993**, *15*, 311–317.
5. Kim, D.H.; Kang, S.Y.; Kim, H.J.; Kim, H.S. Strain rate dependent mechanical behavior of glass fiber reinforced polypropylene composites and its effect on the performance of automotive bumper beam structure. *Compos. Part B Eng.* **2019**, *166*, 483–496. [[CrossRef](#)]
6. Kumar, P.; Garg, A.; Agarwal, B. Dynamic compressive behaviour of unidirectional GFRP for various fibre orientations. *Mater. Lett.* **1986**, *4*, 111–116. [[CrossRef](#)]
7. Shokrieh, M.M.; Omid, M.J. Compressive response of glass–fiber reinforced polymeric composites to increasing compressive strain rates. *Compos. Struct.* **2009**, *89*, 517–523. [[CrossRef](#)]
8. Takeda, N.; Wan, L. Impact compression damage evolution in unidirectional glass fiber reinforced polymer composites. High Strain Rate Effects on Polymer, Metal and Ceramic Matrix Composites and Other Advanced Materials. In *Proceeding of the ASME International Mechanical Engineering Congress and Exposition, San Francisco, CA, USA, 1995*; pp. 109–113.
9. Yuan, J.; Takeda, N. Impact compressive failure of GFRP unidirectional composites. *Sci. Eng. Compos. Mater.* **2000**, *9*, 1–10. [[CrossRef](#)]
10. Christensen, R.M. *Mechanics of Composite Materials*; Dover Publications Inc.: Mineola, NY, USA, 2012.
11. Kolsky, H. An investigation of the mechanical properties of materials at very high rates of loading. *Proc. Phys. Society. Sect. B* **1949**, *62*, 676. [[CrossRef](#)]
12. Janiszewski, J.; Buzantowicz, W.; Baranowski, P. Correction procedure of wave signals for a viscoelastic split Hopkinson pressure bar. *Probl. Mechatron. Armament Aviat. Saf. Eng.* **2016**, *7*, 17–30. [[CrossRef](#)]
13. Chen, W.W.; Song, B. *Split Hopkinson (Kolsky) Bar: Design, Testing and Applications*; Mechanical Engineering Series; Springer: Berlin/Heidelberg, Germany, 2010.
14. Van Sligtenhorst, C.; Cronin, D.S.; Brodland, G.W. High strain rate compressive properties of bovine muscle tissue determined using a split Hopkinson bar apparatus. *J. Biomech.* **2006**, *39*, 1852–1858. [[CrossRef](#)]
15. Sasso, M.; Newaz, G.; Amodio, D. Material characterization at high strain rate by Hopkinson bar tests and finite element optimization. *Mater. Sci. Eng. A* **2008**, *487*, 289–300. [[CrossRef](#)]
16. Dai, F.; Huang, S.; Xia, K.; Tan, Z. Some fundamental issues in dynamic compression and tension tests of rocks using split Hopkinson pressure bar. *Rock Mech. Rock Eng.* **2010**, *43*, 657–666. [[CrossRef](#)]
17. Gorham, D. Specimen inertia in high strain-rate compression. *J. Phys. D Appl. Phys.* **1989**, *22*, 1888. [[CrossRef](#)]
18. Al-Mousawi, M.; Reid, S.; Deans, W. The use of the split Hopkinson pressure bar techniques in high strain rate materials testing. *Proc. Inst. Mech. Eng. Part C J. Mech. Eng. Sci.* **1997**, *211*, 273–292. [[CrossRef](#)]
19. Ravichandran, G.; Subhash, G. Critical appraisal of limiting strain rates for compression testing of ceramics in a split Hopkinson pressure bar. *J. Am. Ceram. Soc.* **1994**, *77*, 263–267. [[CrossRef](#)]
20. Bieler, S.; Weinberg, K. Correction of Wave Signals for PMMA Split Hopkinson Pressure Bar Setups. *PAMM* **2021**, *20*, e202000143. [[CrossRef](#)]
21. Weinberg, K.; Khosravani, M.R.; Thimm, B.; Reppel, T.; Bogunia, L.; Aghayan, S.; Nötzel, R. Hopkinson bar experiments as a method to determine impact properties of brittle and ductile materials. *GAMM-Mitteilungen* **2018**, *41*, e201800008. [[CrossRef](#)]
22. Aghayan, S.; Bieler, S.; Weinberg, K. Determination of the high-strain rate elastic modulus of printing resins using two different split Hopkinson pressure bars. *Mech. Time-Depend. Mater.* **2022**, *26*, 761–773. [[CrossRef](#)]
23. Ninan, L.; Tsai, J.; Sun, C. Use of split Hopkinson pressure bar for testing off-axis composites. *Int. J. Impact Eng.* **2001**, *25*, 291–313. [[CrossRef](#)]
24. Song, B.; Syn, C.; Grupido, C.L.; Chen, W.; Lu, W.Y. A long split Hopkinson pressure bar (LSHPB) for intermediate-rate characterization of soft materials. *Exp. Mech.* **2008**, *48*, 809–815. [[CrossRef](#)]
25. Ren, Z.; Vesjenjak, M. Computational and experimental crash analysis of the road safety barrier. *Eng. Fail. Anal.* **2005**, *12*, 963–973. [[CrossRef](#)]

26. Paul, H.; Ledford, N.; Mohrmann, R.; May, M. Testing of CFRP at High Strain Rates with the Split Hopkinson Tension Bar—Evaluation of Testing Quality. In Proceedings of the ECCM 2016—17th European Conference on Composite Materials, Munich, Germany, 26–30 June 2016.
27. Raj, A.; Nagarajan, P.; Aikot Pallikkara, S. Application of fiber-reinforced rubcrete for crash barriers. *J. Mater. Civ. Eng.* **2020**, *32*, 04020358. [[CrossRef](#)]
28. Tarfaoui, M.; Nème, A.; Choukri, S. Damage kinetics of glass/epoxy composite materials under dynamic compression. *J. Compos. Mater.* **2009**, *43*, 1137–1154. [[CrossRef](#)]

Disclaimer/Publisher’s Note: The statements, opinions and data contained in all publications are solely those of the individual author(s) and contributor(s) and not of MDPI and/or the editor(s). MDPI and/or the editor(s) disclaim responsibility for any injury to people or property resulting from any ideas, methods, instructions or products referred to in the content.